



## Research Article

# Computational analysis of the heat and mass transfer in a casson nanofluid with a variable inclined magnetic field

Toyin Wasu AKAJE<sup>1,\*</sup>, Bakai Ishola OLAJUWON<sup>1</sup>, Musiliu Tayo RAJI<sup>1</sup>

<sup>1</sup>Federal University of Agriculture, Abeokuta, Ogun State, 111101, Nigeria

## ARTICLE INFO

### Article history

Received: 04 May 2021

Revised: 01 August 2021

Accepted: 24 November 2021

### Keywords:

Magnetic Field; Casson  
Nanofluid; Thermo; Thermal  
Diffusion

## ABSTRACT

Investigation of the impacts of thermo and thermal diffusion on a conducting Casson nano liquid with an inclined magnetic field is computationally examined. The partial differential equations that governed the considered flow model are transformed to ordinary highly non-linear derivative equations. The non-dimensional formulated equations are solved using the Spectral Collocation Method (SCM). The method is adopted for various values of dimensionless momentum, heat transfer, and nanoparticle mass distribution. The computed solutions are compared with the existing results for a special limiting case for this study. Also, a graphical illustration of parameters embedded in the flow model is offered for the flow physical dynamical quantities such as the skin coefficient local friction, local temperature gradient, and local species mass gradient. The outcomes revealed that the nano-Casson fluid viscosity is enhanced as the velocity decreases with the rising magnetic field term, whereas heat propagation and mass nanoparticle field is augmented. The species fractional nanofluid is inspired by increasing chemical reactions. Hence, the results of this analysis will assist the chemical industries in monitoring their various activities to prevent reaction inflatable.

**Cite this article as:** Akaje TW, Olajuwon BI, Raji MT. Computational analysis of the heat and mass transfer in a casson nanofluid with a variable inclined magnetic field. Sigma J Eng Nat Sci 2023;41(3):512–523.

## INTRODUCTION

Materials that do not satisfy Newton's law of viscosity and also in linear variance are proportional to the rate of shear strain and synonymous to non-Newtonian fluid. Typical cases of such liquids are condensed milk, tomato muds, and glue. The appropriateness of non-Newtonian fluids over Newtonian fluids is dependent on its valued industrial application like petroleum drilling, polymer engineering,

food manufacturing, and specific separation processes. In addition to that, non-Newtonian fluids models remain on higher pedestals because of their diverse flow behavioural value which has been taken into consideration. Further studies reveal that fluid that emanates from non-Newtonian models are discovered to be more potent than any other non-Newtonian fluids model. This is done because of its accuracy at a higher and lower shear rate. Further, it is known to be of immense use by petroleum engineers in

### \*Corresponding author.

\*E-mail address: akajewasiu@gmail.com

This paper was recommended for publication in revised form by  
Regional Editor Mostafa Safdari Shadloo



the characterization of the cement industry. The fluid is assumed to have a thinning shear with boundless viscosity of zero shear rate and lower yield stress. Among such fluids is Casson fluid which acts like a solid when yield stress is greater than shear stress, and it acts like a liquid when yield stress is lower than the shear stress. Notable cases of the fluid are soap, honey, tomato sauce, jelly and so on. To ensure its functionality, Casson fluid model captures different substances like human blood, plasma, aqueous globulin, fibrinogen, protein etc. and its form chain-like structure called rouleaux. The chain structure acts like a solid plastic that denotes the presence of yield stress in Casson's fluid. According to their submissions, [1] reported on the MHD radiative Casson liquid flows past a stretching power-law sheet with species reaction, the outcomes show that the fixed point velocity point increase with a rise in the non-linear stretching parameters. Meanwhile, the heat transfer and mass species profiles reduce with an enhancing non-linear stretching parameter. The effects of a mass reaction transfer and radiative heat on the Casson MHD flowing liquid over a stretching non-linear plate with suction have been reported that a rise in the value of the magnetic, Casson and suction parameters discourages velocity field and its boundary layer viscosity this in support of Bhim's assertion. [2]. Analysed Casson stagnation MHD flowing fluid through a stretching non-linear plate with dissipating heat. From their findings, it was discovered that the coefficient heat transfer and wall friction increases with rising Casson term values. Other prominent authors that work on the MHD Casson flow can be seen in [3-7].

The basic principle of MHD is straightforward; a uni-directional current is established through an electrically conducting fluid such as seawater. Then, a high intensity magnetic field perpendicular to the current is imposed through the fluid. This combination of orthogonal magnetic field, electric field, and a relative motion of ions results in a Lorentz force with direction defined by the cross product of current and magnetic field vectors [8]. The numerous applications of the magnetic field on the incompressible, conducting viscous fluid has increased its research interest globally. The application includes glass manufacturing control process, magnetic material processing, and purification of crude oil pump application etc. [9] Presented nano-Casson MHD fluid and entropy generation in a permeable shrinking/stretching sheet. The investigation outcomes show that an increase in magnetic and porosity parameters decreases the flow rate profile of the examined flowing fluid. In addition to the existing knowledge. [10]. Studied the impact of energy and species diffusion on the convective MHD flow through an inclined porous medium. It was found that the velocity profile in the cooling case decreases which is in variance and proportional to the magnetic parameter effect. Meanwhile, [11]. Investigated nano-Casson MHD convective heat transport flow past an outstretching surface. An increasing magnetic term was seen to have diminished both the boundary viscosity layer

and the magnitude of the nano-Casson fluid velocity. This agreed well with the observation and findings recorded in [12-16]. With the several works done, little or no study has been carried out on the inclined magnetic field.

When the heat and mass transfer occurs simultaneously in a fluid flow, in many practical and engineering applications the relation between the fluxes and driving potential are more significant. In addition it has been established that an energy flux can be generated not by temperature gradient only but by the composition gradient as well. The Dufour (Diffusion-thermo effect) is the energy generated by a composition gradient, while Soret (thermal-diffusion effect) is the energy generated through the temperature gradient. In general, the Diffusion-thermo effects are of smaller order of magnitude than the effects imposed by Fourier's laws and are often neglected in heat and mass transfer process. Recently in a special case, the Dufour effect was noticed to be of order of considerable magnitude as it cannot be neglected. [17] Reported the significant of their study to investigate the effects of Dufour and Soret on unsteady flow of a Casson fluid in the stagnation point region of rotating sphere and the result proved that Soret and Dufour numbers have tendency to control the thermal and concentration boundary layers. [18]. Examined the effects of Soret and Dufour on MHD Casson fluid over a vertical plate in presence of chemical reaction and radiation. Their result show that concentration found to be decreasing with the increase of Soret number and increasing chemical parameter. Comparison of shooting method with sixth-order of Runge-Kutta technique and Homotopy Adomian's Decomposition method (HADM). [19]. To analyse heat and mass transfer for Soret and Dufour's effect on mixed convection boundary layer flow over a stretching vertical surface in a porous medium filled with a viscoelastic fluid in the presence of magnetic field.

This study aim at investigating the effects of an inclined magnetic field in a nanofluid by taken Casson fluid as the working fluid. [20]. Presented that the spectral collection method serves as the wheel to obtain a solution of the many quasi-linear systems of equations. The proposal has the characteristics of fast convergence and good accuracy as reported in some recent and relevant studies [21-25]. Hence, in this study, the spectral collocation technique is applied.

## MATHEMATICAL ANALYSIS

Considering a Casson nanofluid of steady two-dimensional incompressible flowing liquid over a stretching non-linear plate that is fixed at  $y = 0$  and restrained to  $y > 0$ . The flowing additive liquid is subjected to an unfixed magnetic field  $B(x)$  that is inclined to a stretching plate and is electrically conducting fluid. At this juncture,  $T_\infty$  and  $C_\infty$  remain the significant far stream nano-Casson temperature and chemical species nanoparticle with  $T_\infty > T_w$ . The Brownian movement and thermophoresis of nanoparticles are given attention. The Casson isotropic rheological state model is expressed as reported in [16]:

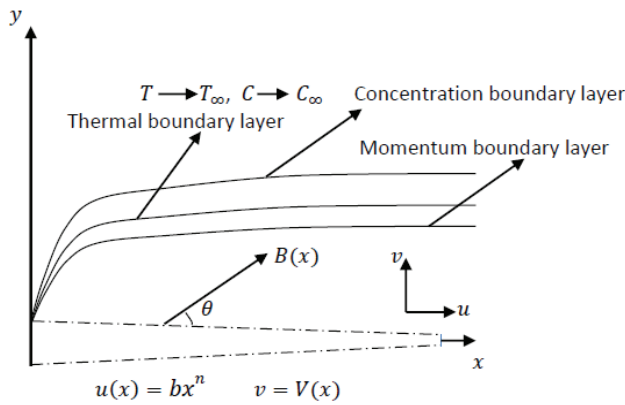


Figure 1. Schematic flow physical coordinate.

$$\tau_{ij} = \begin{cases} \left(\mu_B + \frac{p_y}{\sqrt{2\pi}}\right) 2e_{ij}, & \pi > \pi_c \\ \left(\mu_B + \frac{p_y}{\sqrt{2\pi_c}}\right) 2e_{ij}, & \pi < \pi_c \end{cases} \quad (1)$$

Here,  $\mu_B$  denotes plastic non-Newtonian dynamical viscosity,  $p_y$  defines the fluid yield stress,  $\pi$  represents the self-deformation rate components product, that is  $\pi = e_{ij} e_{ij}$  in which  $e_{ij}$  is the deformation components rate  $(i, j)^{th}$  with  $\pi_c$  serves as the  $\pi$  based critical value for the non-Newtonian formulation. The governing equations for the flow conservation of mass, velocity module, energy component, and dimensional mass are respectively satisfied as:

$$\frac{\partial u}{\partial x} + \frac{\partial v}{\partial y} = 0 \quad (2)$$

$$u \frac{\partial u}{\partial x} + v \frac{\partial u}{\partial y} = v \left(1 + \frac{1}{\beta}\right) \frac{\partial^2 u}{\partial y^2} - \frac{\sigma B^2(x)}{\rho} u \sin^2 \varphi \quad (3)$$

$$u \frac{\partial T}{\partial x} + v \frac{\partial T}{\partial y} = \frac{k}{\rho c_p} \frac{\partial^2 T}{\partial y^2} + \tau \left[ D_B \left( \frac{\partial C}{\partial y} \frac{\partial T}{\partial y} \right) + \frac{D_T}{T_\infty} \left( \frac{\partial T}{\partial y} \right)^2 \right] + \frac{\mu}{\rho c_p} \left(1 + \frac{1}{\beta}\right) \left( \frac{\partial u}{\partial y} \right)^2 + \frac{\sigma B^2(x)}{\rho c_p} u^2 \sin^2 \varphi + \frac{D_{mK(x)}}{C_s C_p} \frac{\partial^2 C}{\partial y^2} - \frac{1}{\rho c_p} \frac{\partial q_r}{\partial y} \quad (4)$$

$$u \frac{\partial C}{\partial x} + v \frac{\partial C}{\partial y} = D_B \frac{\partial^2 C}{\partial y^2} + \frac{D_T}{T_\infty} \frac{\partial^2 T}{\partial y^2} + \frac{D_{mK(x)}}{T_m} \frac{\partial^2 T}{\partial y^2} - K(x)(C - C_\infty) \quad (5)$$

At this point,  $u$  and  $v$  are the modules velocity in  $x$  and  $y$  coordinates correspondingly. Going by this postulation,  $c_p$  indicates specific,  $v$  stands for the liquid kinematic viscosity,  $\rho$  represents working fluid density,  $\beta = \mu_B \sqrt{\frac{2\pi_c}{p_y}}$  is the non-Newtonian or Casson term measure,  $\sigma$  depicts fluid electrical conductivity,  $T$  is the temperature,  $k$  signifies thermal conductivity,  $T_w$  connotes the constant plate temperature,  $\frac{k}{\rho c_p}$  means base fluid heat diffusivity,  $\tau = \frac{(\rho c)_p}{(\rho c)_f}$  defines

the proportional ratio of heat capacity nanoparticle to heat capacity of the working liquid,  $D_B$  describes Brownian coefficient diffusion while,  $D_T$  expresses thermophoretic coefficient diffusion,  $K(x)$  denotes variable reaction rate and  $B_0$  represents magnetic field inclined strength. Magnetic field induction is taken to be insignificant. An applied magnetic field defined as  $B = B_0 x^{\frac{n-1}{2}}$  is assumed with constant  $B_0$ .

The boundary conditions proportional to a non-linear stretching sheet is presented as:

$$u = U = bx^n, v = V(x), T = T_w, C = C_w \text{ at } y = 0 \quad (6)$$

$$u \rightarrow 0, T \rightarrow T_\infty, C \rightarrow C_\infty \text{ as } y \rightarrow y_\infty \quad (7)$$

where  $T_w = T_o + T_o x^m$  is the temperature at the sheet,  $C_w = C_o + C_o x^t$  is the concentration at the sheet,  $b$  represents stretching plate velocity with  $b > 0$  denoting plate elongation and  $b < 0$  depicts plate shrinking. The power index velocity for the stretching plate velocity is  $n$ ,  $V(x)$  is the velocity of the suction,  $t$  is concentration power index parameter,  $m$  is the power index for temperature while,  $V_o$ ,  $C_o$  and  $T_o$  are constants and heat flux radiation is  $q_r$ .

Adopting the approximated Rosseland definition for the radiation Brewster (1972)  $q_r = \frac{-4\sigma^* \partial T^4}{3k' \partial y}$  is obtained, where  $\sigma^*$  stands for the Stefan-Boltzmann constant and  $k'$  denotes mean coefficient absorption. Taken that the flow temperature varies such that  $T^4$  may be in Taylor's series expansion. Expanding  $T^4$  about  $T_\infty$  and neglect larger-order terms to arrive at  $T^4 = 4T_\infty^3 T - 3T_\infty^4$ .

Introducing the following transformations:

$$\eta = y \sqrt{\frac{b(n+1)}{2v} x^{n-1}}, \quad u = bx^n f'(\eta), \quad v = -\sqrt{\frac{bv(n+1)}{2}} x^{n-1} \quad (8)$$

$$\left[ f(\eta) + \frac{n-1}{n+1} \eta f'(\eta) \right], \quad \theta(\eta) = \frac{T-T_\infty}{T_w-T_\infty}, \quad \phi(\eta) = \frac{C-C_\infty}{C_w-C_\infty}$$

By substituting (8) in (3), (4) and (5), we obtained the reduced governing equations as:

$$\left(1 + \frac{1}{\beta}\right) f'''' + f f'' - \frac{2n}{n+1} f'^2 - \frac{2M}{n+1} f' \sin^2 \varphi = 0 \quad (9)$$

$$\left(1 + \frac{1}{R}\right) \frac{1}{P_r} \theta'' + f \theta' - \frac{2m}{n+1} f' \theta + N_b \theta''^2 + \left(1 + \frac{1}{\beta}\right) E_c f''^2 + \frac{2M}{n+1} f'^2 \sin^2 \varphi + D_f \phi'' = 0 \quad (10)$$

$$\frac{1}{S_c} \phi'' + f \phi' - \frac{2t}{n+1} \phi f' - \frac{Y}{n+1} \phi + \frac{N_t}{N_b} \theta'^2 + S_r \theta'' = 0 \quad (11)$$

With parameters:

$$M = \frac{\sigma B_0^2}{\rho b}, R = \frac{3kk'}{16\sigma^* T_\infty^3}, K(x) = \frac{bx^{n-1}L}{V_0}, Y = \frac{2L}{V_0}, D_f = \frac{D_m k_T (C_w - C_\infty)}{C_s C_p (T_w - T_\infty)},$$

$$S_r = \frac{D_m k_T \rho c_p (T_w - T_\infty)}{T_m k (C_w - C_\infty)}, S_c = \frac{v}{D}, v = \frac{\mu}{\rho} \quad (12)$$

$D_f$  is the Dufour number,  $S_r$  denotes the soret term,  $M$  is the magnetic term,  $P_r$  represents Prandtl number,  $D$  implies the coefficient of species diffusion,  $K(x)$  varying rate of reaction,  $Y$  is a reaction species,  $S_c$  is Schmidt number and  $L$  is reference length.

The boundary conditions are expressed as:

$$f(0) = S, f'(0) = 1, \theta(0) = 1, \phi(0) = 1$$

$$f'(\infty) = 0, \theta(\infty) = 0, \phi(\infty) = 0 \quad (13)$$

where the prime denotes the derivative with respect to  $\eta$ , and  $S = \frac{V_0}{(\frac{bv(n+1)}{2})^{\frac{1}{2}}}$  is the suction term.

The engineering bodily measures of attention are the coefficient of skin friction (wall shear stress rate), the Nusselt number (heat transfer gradient), and the Sherwood number (mass transfer gradient).

The skin local friction  $C_{f_x}$ , Nusselt local  $Nu_x$  and Sherwood local  $Sh_x$  numbers are described as

$$C_{f_x} = \frac{\tau_w}{\frac{\rho u_\infty^2}{2}} = \left(\frac{2(n+1)}{Re}\right)^{\frac{1}{2}} \left(1 + \frac{1}{\beta}\right) f''(0), Re = \frac{bx^{(n+1)}}{v}, Nu = -\left(\frac{(n+1)bx^{(n+1)}}{2v}\right)^{\frac{1}{2}} \theta'(0)$$

$$= -\left(\frac{Re(n+1)}{2}\right)^{\frac{1}{2}} \theta'(0), Sh = -\left(\frac{(n+1)bx^{(n+1)}}{2v}\right)^{\frac{1}{2}} \phi'(0)$$

$$= -\left(\frac{Re(n+1)}{2}\right)^{\frac{1}{2}} \phi'(0)$$

where  $Re = \frac{bx^{(n+1)}}{v}$  is the Reynolds local number.

### Computational Solution Technique

The Chebyshev spectra-collocation method is employed to determine a computational solution for the present system of quasilinear differential Eqs. (9)–(11) with the boundary condition (13). Due to its numerous advantages over others methods like Kudryashov method by Ali et al. [26], Variational Iteration algorithm-I by Ahmad [27] and Riccati transformation by Bazighifan and Ahmad [28], such as high accuracy, efficiency and ability to solve both nonlinear and linear ODEs/ PDEs systems of equations. Ehrenstein and Peyret [29] described the Chebyshev  $n$ th-order polynomial defined by  $T_n(\xi); n \geq 0$  as

$$T_n(\xi) = \cos(n \cos^{-1} \xi); \quad -1 \leq \eta \leq 1 \quad (15)$$

The recursive formula is written as  $T_{n+1} = 2xT_n(x) - T_{n-1}(x); n \geq 1$ . The range of the flow  $[0, \infty)$  is approximately taken as  $[0, L]$  in other to introduce CSCM. The far domain of the boundary is  $L$  and the value of  $L$  defines the far stream convergence

of the solution. Therefore, the range  $[0, L]$  is converted to the range  $[-1, 1]$  using the following algebraic definition

$$\xi = \frac{2\eta}{L} - 1, \quad \xi \in [-1, +1] \quad (16)$$

Let assume that  $f(\eta), \theta(\eta)$  and  $\phi(\eta)$  is the unknown basis function  $T_k(\xi)$ . to be approximated.

$$\left. \begin{aligned} f(\eta) &= \sum_{k=0}^N a_k T_k(\eta) \\ \theta(\eta) &= \sum_{k=0}^N b_k T_k(\eta) \\ \phi(\eta) &= \sum_{k=0}^N c_k T_k(\eta) \end{aligned} \right\} \quad (17)$$

where  $a_k, b_k$  and  $c_k$  are unknown coefficients to be obtained? Therefore, to have the residual equations, Eqn. (20) used on the governing equations (11)- (13), where the coefficient  $a_n, b_n$  and  $c_n$  are taken to reduce the residual error as low as possible between the considered range. Chebyshev collocation is used which is expressed according to Ehrenstein and Peyret [29].

$$\eta_j = \cos\left(\frac{\pi j}{N}\right), \quad j = 0, \dots, N. \quad (18)$$

This generates a  $3N + 3$  system of algebraic equations along with the  $3N + 3$  coefficients  $a_k, b_k$  and  $c_k$  to be determined. An iterative Newton's technique follow by Finlayson [30] is employed on the resulting residues  $N = 30$ . Hence, the boundary value algorithm is established in Mathematica software to obtain the computational results for the problem.

### RESULTS AND DISCUSSION

A detailed analysis is numerically carried out by using the spectral collocation method to gain a perspective behaviour of physical thermodynamic implication for different fluid terms. The fluid parameters include magnetic ( $M$ ), Casson ( $\beta$ ), radiation ( $R$ ), the thermal index ( $m$ ), concentration ( $t$ ), Schmidt parameters measures. In addition, Schmidt ( $S_c$ ), Prandtl ( $P_r$ ), Dufour ( $D_f$ ) and Soret number ( $S_r$ ). To cap it up, a discussion of the shear stress at the wall, gradient of heat transfer and gradient of mass transfer are comprehensively done. The data for the discussion is offered in tables 1-4 and graphically presented in Figures 1-21 for proper illustrations of the results.

In Figure 2, the researcher noticed a reduction in velocity profile fluid which is in contrast to the magnetic field that often increases. The notice is connected to the point that the application of an inclined magnetic field has a possibility of creating a drag known as the Lorenz force that

**Table 1.** Assessment of  $-f'''(0)$  for various computed results of  $n$  when  $t=0$ ,  $n=1$ ,  $Sc=0.22$ ,  $Pr=inf$ ,  $b=10.8$ ,  $S=0.0$ ,  $k=0$ ,  $m=0$ ,  $M=0$ ,  $Df=Sr=Ec=0$ 

<b>M=0, n1=1, b=10.8, Pr=inf, t=0, m=0, Sc=0.22, S=0.0, c=0</b>		
<b><math>-f'''(0)</math></b>		
<b>N</b>	<b>Ullah et. al. [5]</b>	<b>Bhim [31] Present</b>
0.0	0.6276	0.627554 0.6269847
0.2	0.7668	0.766835 0.7655849
0.5	0.8896	0.889537 0.8755736
1	1.0	1.000001 1.0000214
3	1.1486	1.148604 1.1479463
10	1.2349	1.234882 1.2336775
100	1.2768	1.276784 1.2758468

**Table 2.** Assessment of Nassult local number  $-\theta'(0)$  for various computed results of  $n$  when  $Sc=0.22$ ,  $m=0$ ,  $t=0$ ,  $R=inf$ ,  $Pr=1$  and  $5$ ,  $b=10.8$ ,  $n=0.2$ ,  $M=0$ ,  $S=0.0$ ;  $k=0$ ;  $Df=Sr=Ec=0$ ;

<b>t=0, k=0, S=0.0, n=0.2, Sc=0.22, m=0, R=inf, M=0; b=10.8</b>			<b>m=0, t=0, R=inf, b=10.8, n1=0.2, M=0, Sc=0.22, S=0.0, k=0</b>	
<b><math>-\theta'(0), Pr=1,</math></b>			<b><math>-\theta'(0), Pr=5,</math></b>	
<b>n</b>	<b>Bhim [31]</b>	<b>Present</b>	<b>Bhim [31]</b>	<b>Present</b>
0.2	0.610203	0.610316402311	1.607799	1.607897754510
0.5	0.595204	0.586301145202	1.586794	1.586698457731
1.5	0.574736	0.573864711390	1.557705	1.557668595746
3.0	0.564671	0.564596813304	1.543190	1.542799465549

**Table 3.** Results assessment for reducing Nassult number  $-\theta'(0)$  for various computed values of  $Pr$  when  $S=0.0$ ,  $Pr=0.7$ ,  $Sc=0.22$ ,  $b=10.8$ ,  $n=1$ ,  $M=0$ ,  $m=0$ ,  $R=inf$ ,  $t=0$ ,  $k=0$ ,  $Df=Sr=Ec=0$ 

<b>Pr=0.7, R=inf, t=0, m=0, Sc=0.22, S=0.0, M=0, n=1, b=10.8, k=0, Df=Sr=Ec=0</b>		
<b><math>-\theta'(0), Pr=1,</math></b>		
<b>Pr</b>	<b>Bhim [31]</b>	<b>Present</b>
0.7	0.454049789	0.453577403117
2	0.977361122	0.976944864739
7	1.895415848	1.889960463381
20	3.353940663	3.352753126902
70	6.462331549	6.459063552380

usually serves as a resistance to the flow of fluid in the boundary layer. In Figures 3 and 4, a show of increase in the heat diffusion and nanoparticle mass transfer field which is of equal value to the increase noticed in the magnetic parameters is presented and it results in the thickness of the corresponding boundary film. Figure 5 illustrates the influence of the Casson term on the flow momentum distribution. As clearly observed, an upsurge in the Casson term

resulted in a decline in both the flow rate profile and the corresponding boundary film viscosity. However, Figures 6 and 7 present the temperature, nanoparticle mass species diffusion profile and the equivalent flow limiting layer viscosity increases together with a rise in the Casson term. Figures 8 and 9 exhibits the effects of stretching of index term on the velocity field and nanoparticle chemical species profile, therefore a boost in the stretching index parameter

**Table 4.** Impact of different bodily terms on the Skin-friction, Nusselt and Sherwood numbers

$M$	$n$	$N_t$	$m$	$R$	$Sc$	$t$	$Df$	$Sr$	$Ec$	$f''(0)$	$-\theta'(0),$	$\phi'(0),$
0										-0.772363	1.84338	0.191959
1.0										-1.000000	1.18798	0.215725
2.0										-1.18228	0.638293	0.226261
	0.5									-1.01005	1.20859	0.267953
	1.0									-1.00000	1.18798	0.215725
	2.0									-0.989537	1.17392	0.154099
		0.1								-1.21825	1.23542	0.21033
		0.6								-1.21825	1.02132	-0.05269
		1.1								-1.21825	0.85766	-0.25563
			0.5							-1.21825	2.09596	0.153663
			1.0							-1.21825	2.36512	0.141997
			2.0							-1.21825	2.84248	0.119606
				0.5						-1.21825	0.53887	0.255228
				1.0						-1.21825	0.738875	0.242282
				1.5						-1.21825	0.848211	0.235175
					0.2					-1.21825	2.36222	0.149873
					0.4					-1.21825	2.37146	0.110594
					0.6					-1.21825	2.3888	0.0416495
						0.5				-1.21825	2.37357	0.111693
						1.0				-1.21825	2.36512	0.141997
						2.0				-1.21825	2.34878	0.200811
							0			-1.21825	1.24708	0.209047
							0.5			-1.21825	1.18657	0.215411
							1.0			-1.21825	1.12052	0.221663
								0.4		-1.21825	1.23898	0.179486
								0.8		-1.21825	1.24372	0.138042
								1.2		-1.21825	1.24853	0.0962119
									0	-1.21825	1.33454	0.205991
									0.5	-1.21825	0.836984	0.225279
									1.0	-1.21825	0.334356	0.238524

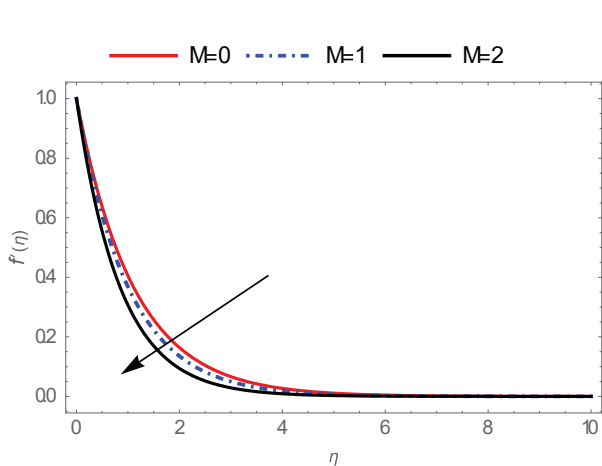


**Figure 2.** magnetic field (M) effect on the velocity field.

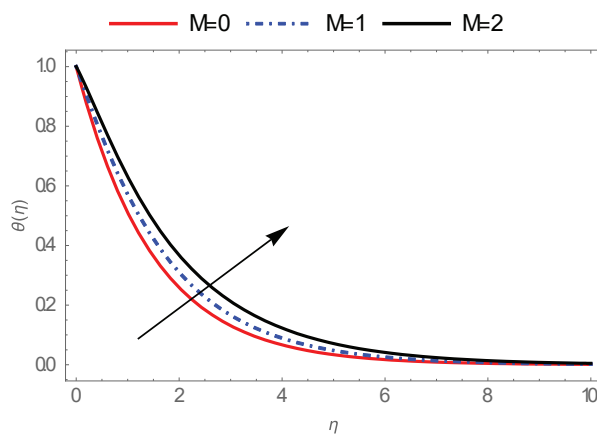


**Figure 3.** Effects of the magnetic field (M) on the temperature field.

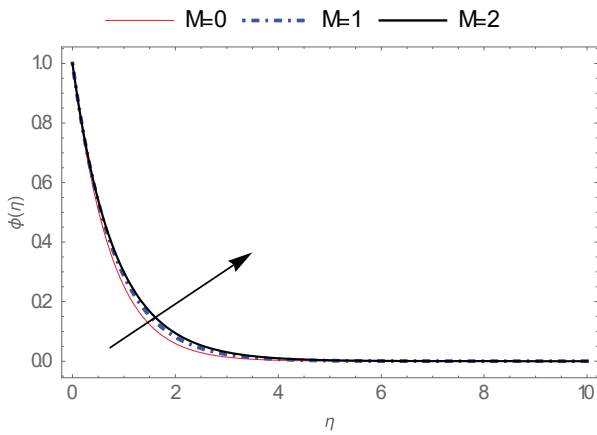


**Figure 4.** Impacts of the magnetic field ( $M$ ) on the nanoparticle concentration field.

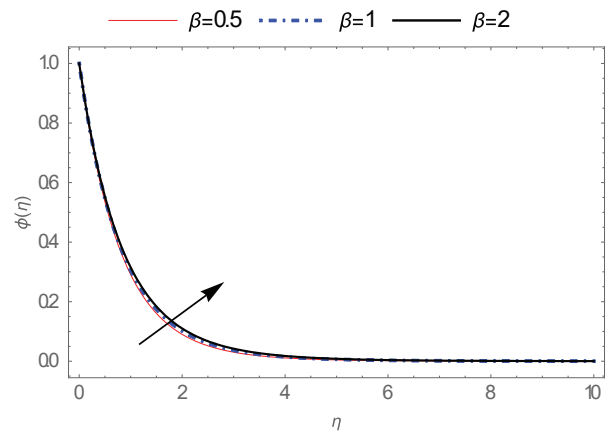


**Figure 7.** Impacts of Casson term ( $\beta$ ) on the nanoparticle species profile.

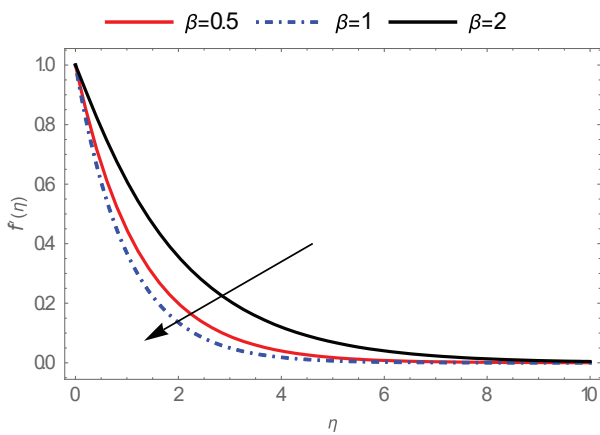


**Figure 5.** Effects of Casson term ( $\beta$ ) on the velocity distribution.

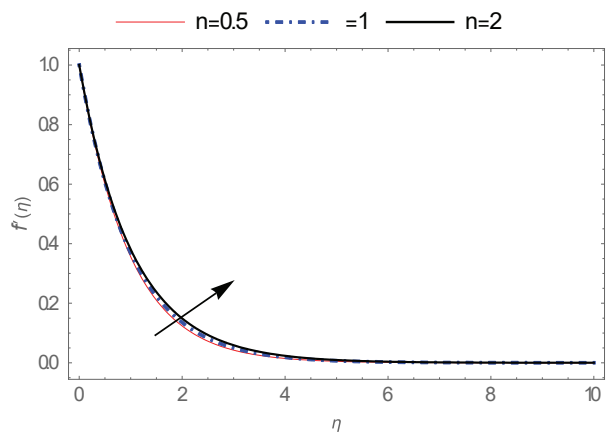


**Figure 8.** Effects of stretching index term ( $n$ ) on the velocity distribution.

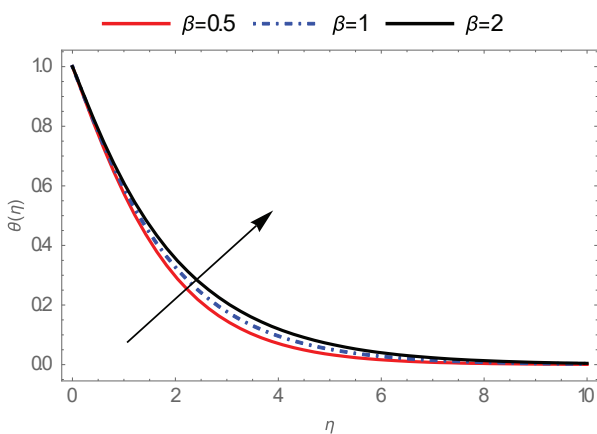


**Figure 6.** Influences of Casson term ( $\beta$ ) on the heat distribution.

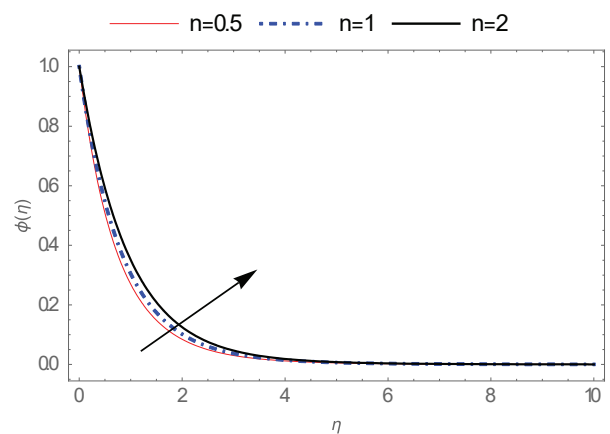


**Figure 9.** Impacts of stretching index term ( $n$ ) on the nanoparticle concentration profile.

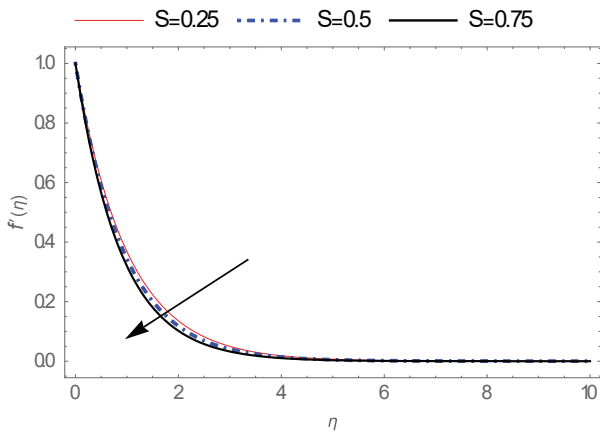


**Figure 10.** Influences of the suction term ( $S$ ) on the velocity field.

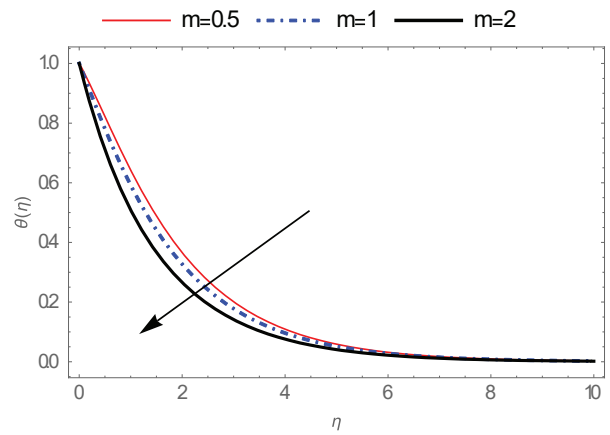


**Figure 13.** Impacts of heat index term ( $m$ ) on the temperature distribution.

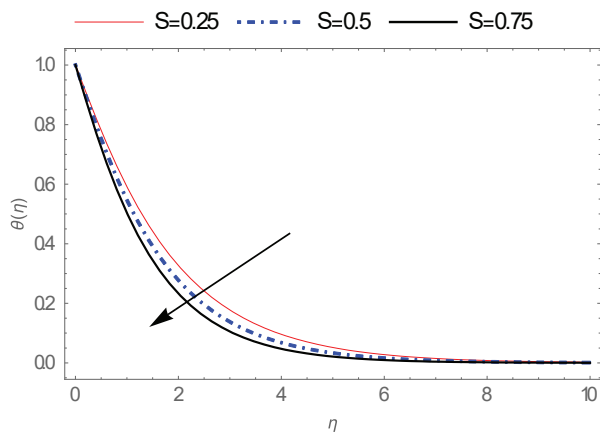


**Figure 11.** Effects of the suction term ( $S$ ) on the temperature field.

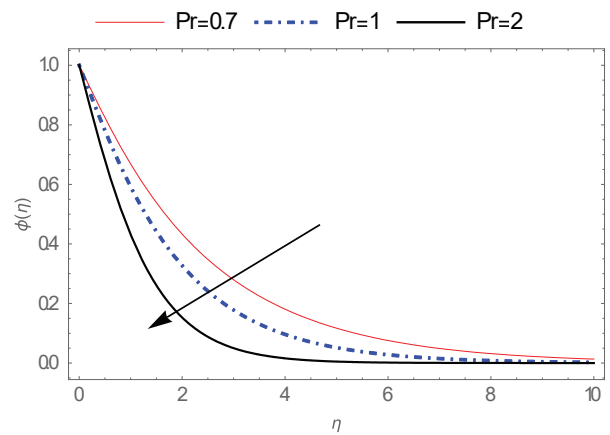


**Figure 14.** Impacts of Prandtl number ( $P_r$ ) on the nanoparticle concentration profile.

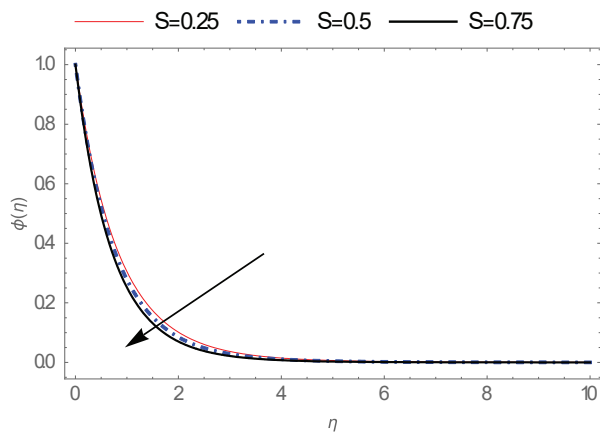


**Figure 12.** Effects of the suction term ( $S$ ) on the nanoparticle concentration profile.

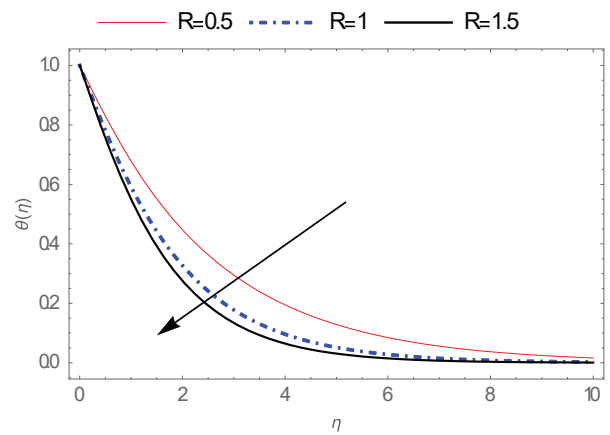


**Figure 15.** Influences of radiation term ( $R$ ) on the heat transfer.

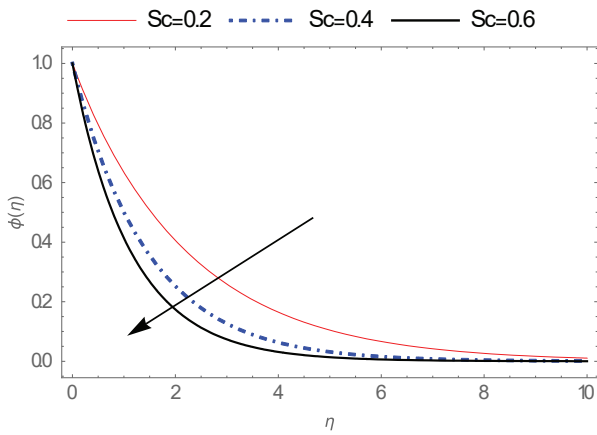


**Figure 16.** Effects of Smidth parameter ( $S_c$ ) on the nanoparticle concentration profile.

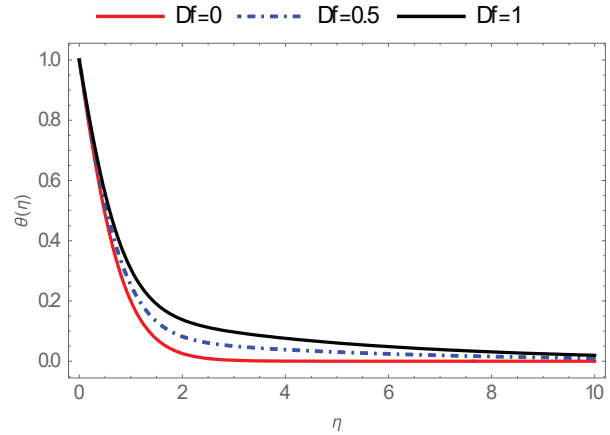


**Figure 19.** Effects of Dufour number ( $D_f$ ) on the temperature profile.

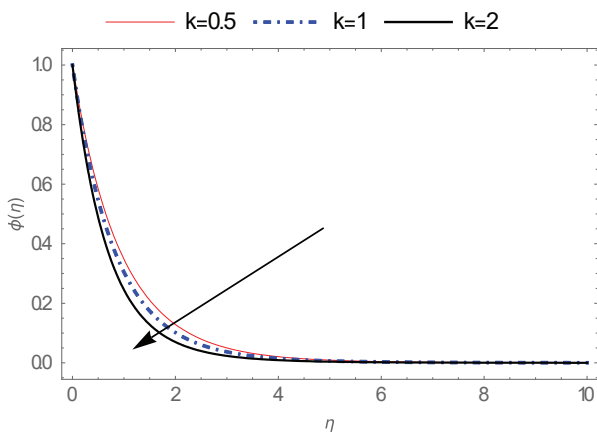


**Figure 17.** Influences of the chemical reaction ( $k$ ) on the nanoparticle mass transfer field.

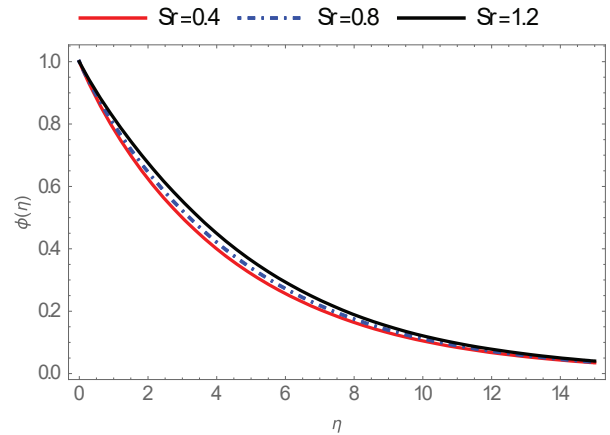


**Figure 20.** Effects of Soret number ( $S_r$ ) on the nanoparticle mass species field.

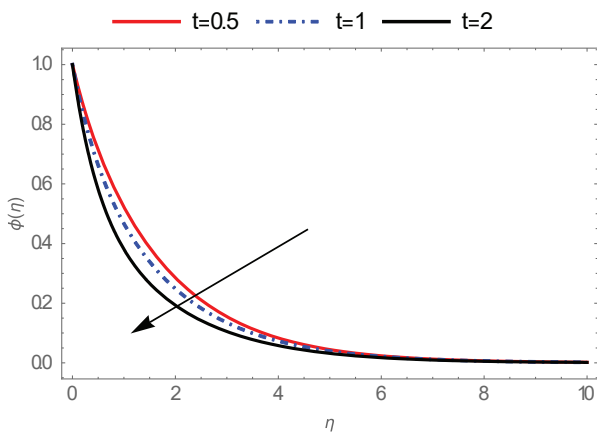


**Figure 18.** Effects of concentration index parameter ( $t$ ) on the nanoparticle concentration profile.

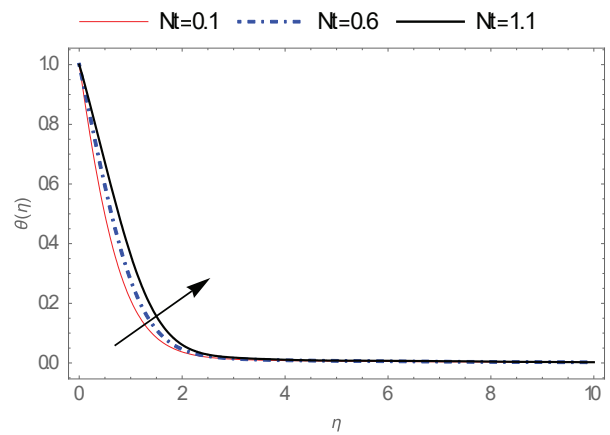


**Figure 21.** Effects of thermophoresis term ( $N_t$ ) on the heat distribution.

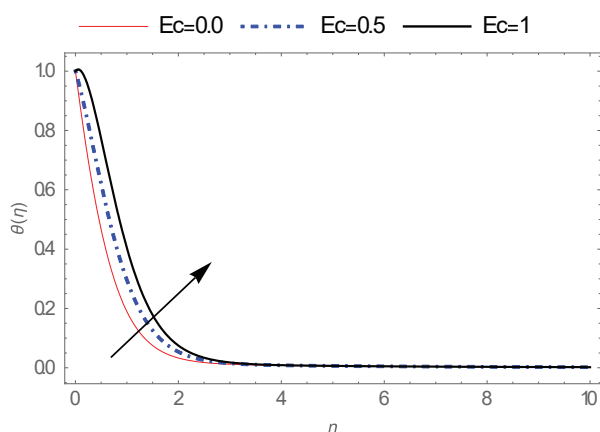


**Figure 22.** Impacts of Eckert number ( $E_c$ ) on the heat transfer field.

causes an increase in velocity, heat transfer, nanoparticle profiles and corresponding boundary layer thickness.

Velocity and concentration nanoparticle distributions decrease respectively in figures 10-12 with increasing in the suction term that leads to diminishing resultant boundary layer viscosity. The illustration of the thermal index parameter ( $m$ ) is presented in Figure 13 on heat transfer profile and it is seen that temperature reduces as the thermal index term rises with a diminish in the equivalent boundary thermal layer viscosity. In Figures 14 and 15, the behavioural show of the thermal radiation and Prandtl number on the thermal diffusion profiles is plotted and presented. Enhanced thermal radiation values and Prandtl number cause a reduction in the temperature fields and thereafter causes a corresponding decrease in the thermal layer thickness. Furthermore, the decrease in nanoparticle mass transfer profiles and corresponding mass boundary film thickness is observed in Figures 16-18 for different values of Schmidt  $S_c$ , chemical reaction  $K$ , and concentration index parameters  $t$ . An increase in the Dufour number ( $D_f$ ) serves because of the increase in fluid temperature, (see figure 19). The Soret number ( $S_r$ ) impact on the nanoparticle species transfer profile is displayed in figure 20. This displays that the nanoparticle concentration field rises by an increasing value of Soret number and thus causes an increasing thickness of thermal boundary film. In figures 21 and 22, a display of solution of heat distributions across the layer boundary thickness for diverse values of dimensionless thermophoresis term ( $N_t$ ) and Eckert number ( $E_c$ ) is made. Similarly, we notice that an increase in this thermophoresis and Eckert number leads to a rise in the thermal fluid heat transfer.

## CONCLUSIONS

The paper investigates the effect of thermal and thermo-diffusion on a Casson nano liquid with an inclined magnetic

field. The partial derivative model equations which control the flow problems are transmuted by similarity transformation to an ordinary system of derivative equations. The numerical solution derived from these studies is arrived at by using the spectral collocation method for the complete solution of the flow rate, heat transfer and concentration nanoparticle distributions. These submissions are graphically presented to enable easy access for different values of fluid embedded terms that are subsumed in the flow model. The under-listed outcomes, among others, reveal that:

- \*introduction of an inclined magnetic field decreases the flow velocity distribution of the fluid flow because it creates a drag force known as the Lorenz force that is capable of resisting the flow dynamics.

- \* The concentration boundary film viscosity increases as the Soret number ( $S_r$ ) is increased.

- \*The heat boundary film viscosity increases as the Dufour number ( $D_f$ ) is enhanced.

- \* The temperature boundary film tends to decline with an augmentation in the Prandtl number due to strong ambient heat diffusion.

Hence, the study is useful to the chemical and thermal sciences for the accurate prediction of their activities as well as improving industrial productivity. Therefore, an extension of this study is encouraged to fluid flow in a concentric cylinder under isothermal conditions.

## ACKNOWLEDGEMENTS

This work was supported by the Research Fund of the Bursa Uludag University, Project Number OUAP(F)-2019/9. The authors would like to thank for this support.

## AUTHORSHIP CONTRIBUTIONS

Authors equally contributed to this work.

## DATA AVAILABILITY STATEMENT

The authors confirm that the data that supports the findings of this study are available within the article. Raw data that support the finding of this study are available from the corresponding author, upon reasonable request.

## CONFLICT OF INTEREST

The author declared no potential conflicts of interest with respect to the research, authorship, and/or publication of this article.

## ETHICS

There are no ethical issues with the publication of this manuscript.

## REFERENCES

- [1] Motahar Reza NS, Chahal R. Radiation effect on MHD casson fluid flow over a power-law stretching sheet with chemical reaction. *Int J Chem Eng* 2016;10:585–590.
- [2] Medikare M, Joga S, Chidem KK. MHD stagnation point flow of a casson fluid over a nonlinearly stretching sheet with viscous dissipation. *Am J Comput Math* 2016;6:37–48. [\[CrossRef\]](#)
- [3] Khalid S, Kamal AM, Rasheed U, Farooq S, Hussain S, Waqas H. Buoyancy and the chemical reaction effects on MHD flow of casson fluids through a porous medium due to a porous shrinking sheet. *J Appl Environ Biol Sci* 2017;7:154–165.
- [4] Akbar NS. Influences of magnetic field on peristaltic flow of a casson fluid in an asymmetric channel: Application in crude oil refinement. *J Magn Mater* 2015;378:320–326. [\[CrossRef\]](#)
- [5] Bhattacharyya K, Hayat T, Alsaedi A. Analytic Solution for magneto hydrodynamic boundary layer flow of casson fluid over a stretching/shrinking sheet with wall mass transfer. *Chin Phys B* 2013;22:024702. [\[CrossRef\]](#)
- [6] Hassan W, Rafique S, Khalid S, Ahmad F, Hussain S. Thermal radiation effects on unsteady MHD flow of Casson fluids through porous medium over a shrinking sheet. *J Appl Environ Biol Sci* 2017;7:201–209.
- [7] Ullah I, Shafie S, Khan I. Effects of slip condition and Newtonian heating on MHD flow of Casson fluid over a nonlinearly stretching sheet saturated in a porous medium. *J King Saud Univ Sci* 2017;29:250–259. [\[CrossRef\]](#)
- [8] Al-Hababeh OM, Al-Saqqa M, Safi M, Abo Khater T. Review of magnetohydrodynamic pump applications. *Alex Eng J* 2016;55:1347–1358. [\[CrossRef\]](#)
- [9] Qing J, Bhatti MM, Abbas AM, Rashidi MM, Ali EM. Entropy generation on MHD Casson nanofluid flow over a porous stretching/shrinking surface. *Entropy* 2016;18:123. [\[CrossRef\]](#)
- [10] Jhansi Rani J, Ramana Reddy GV, Ramana Rurthy CV, Ramana Murthy MV. Heat and mass transfer effect on MHD free convection flow over an included plate embedded in a porous medium. *Int J Chem Sci* 2015;13:1998–2016.
- [11] Haq UR, Nadeem S, Khan HZ, Okedayo GT. Convective heat transfer and MHD effects on Casson nanofluid flow over a shrinking sheet. *Centr Eur J Phys* 2014;12:862–871. [\[CrossRef\]](#)
- [12] Mustafa M, Khan JA. Model for the flow of Cassonnanofluid past a non-linearly stretching sheet considering magnetic field effects. *AIP Adv* 2015;5:077148. [\[CrossRef\]](#)
- [13] Makanda G, Shaw S, Sibanda P. Diffusion of chemically reactive species in Casson fluid flow over an unsteady stretching surface in porous medium in the presence of a magnetic field. *Math Probl Eng* 2015;2015:724596. [\[CrossRef\]](#)
- [14] Haroun NA, Sibanda PM, Motsa SS. On unsteady MHD mixed convection in a nanofluid due to a stretching/shrinking surface with suction/injection using the spectral realization method. *Bound Val Probl* 2015;2015:1–17. [\[CrossRef\]](#)
- [15] Nandy SK. Analytical solution of MHD stagnation-point flow and heat transfer of Casson fluid over a stretching sheet with partial slip. *Int Sch Res Notices* 2013;2013:108264. [\[CrossRef\]](#)
- [16] Nadeem S, Haq RU, Akbar NS. MHD three-dimensional boundary layer flow of Casson nanofluid past a linearly stretching sheet with convective boundary condition. *IEEE Trans Nanotechnol* 2014;13:109–115. [\[CrossRef\]](#)
- [17] Pushpalatha K, Sugunamma V, Ramana Reddy JV, Sandeep N. Dufour and Soret effects on unsteady flow of a Casson fluid in the stagnation point region of a rotating sphere. *Middle East J Sci Res* 2016;24:1141–1150.
- [18] Reddy NA, Janardhan K. Soret and dufour effects on MHD casson fluid over a vertical plate in presence of chemical reaction and radiation. *Int J Curr Res Rev* 2017;9:55–61.
- [19] Gbadeyan JA, Idowu AS, Ogunsola AW, Agboola OO, Olanrewaju PO. Heat and mass transfer for Soret and Dufour's effect on mixed convection boundary layer flow over a stretching vertical surface in a porous medium filled with a viscoelastic fluid in the presence of magnetic field. *Global J Sci Front Res* 2011;11:97–114.
- [20] Yasong S, Jing M, Benwen L, Zhixiong G. Thermal analysis of a convective-radiative fin with temperature-dependent properties by the collocation spectral method. In: Jaluria Y, Guo Z, editors. *ICHMT International Symposium on Advances in Computational Heat Transfer*; 2015 May 25-29; New Brunswick: Begell House; 2015. pp. 1–17.
- [21] Saedodin S, Barforoush MSM. Comprehensive analytical study for convective-radiative continuously moving plates with multiple non-linearities. *Energy Convers Manag* 2014;8:160–168. [\[CrossRef\]](#)
- [22] Zeng FH, Ma HP, Liang D. Energy-conserved splitting spectral methods for two dimensional Maxwell's equations. *J Comput Appl Math* 2014;265:301–321. [\[CrossRef\]](#)
- [23] Najafi M, Hejranfar K, Efahanian V. Application of a shock-fitted spectral collocation method for computing transient high-speed inviscid flows over a blunt nose. *J Comput Phys* 2014;257:954–980. [\[CrossRef\]](#)
- [24] Ma J, Li BW, Howell JR. Thermal radiation heat transfer in one- and two-dimensional enclosures using the spectral collocation method with full spectrum k-distribution model. *Int J Heat Mass Transf* 2014;71:35–43. [\[CrossRef\]](#)

- [25] Li GU, Ma J, Li BW. Collocation spectral method for the transient conduction radiation heat transfer with variable thermal conductivity in two-dimensional rectangular enclosure. *ASME J Heat Transf* 2015;137:032701. [\[CrossRef\]](#)
- [26] Akbar MA, Akinyemi L, Yao SW, Jhangeer A, Rezazadeh H, Khater MM, et al. Soliton solutions to the Boussinesq equation through sine-Gordon method and Kudryashov method. *Results Phys* 2021;25:104228. [\[CrossRef\]](#)
- [27] Ahmad H. Variational iteration algorithm-I with an auxiliary parameter for wave-like vibration equations; *J Low Freq Noise Vib Act Control* 2019;38:1113–1124. [\[CrossRef\]](#)
- [28] Bazighifan O, Ahmad H. New oscillation criteria for advanced differential equations of fourth order. *Mathematics* 2020;8:728. [\[CrossRef\]](#)
- [29] Zeng FH, Ma HP, Liang D. Energy-conserved splitting spectral methods for two dimensional maxwell's equations. *J Comput Appl Math* 2014;265:301–321. [\[CrossRef\]](#)
- [30] Najafi M, Hejranfar K, Efahanian V. Application of a shock-fitted spectral collocation method for computing transient high-speed inviscid flows over a blunt nose. *J Comput Phys* 2014;257:954–980. [\[CrossRef\]](#)
- [31] Kala B. The effect of chemical reaction and thermal radiation on magnetohydrodynamiccasson fluid flow over non-linearly stretching surface with suction. *Asian Res J Math* 2017;2:1–23. [\[CrossRef\]](#)